Smart Materials and
Structures

PAPER

Influence of mechanical layout of shape memory alloy damping inerter (SDI) systems for vibration control

To cite this article: Ruifu Zhang *et al* 2021 *Smart Mater. Struct.* **30** 085021

Smart Mater. Struct. 30 (2021) 085021 (15pp)
https://doi.org/10.1088/1361-665X/ac0b4c

Influence of mechanical layout of shape memory alloy damping inerter (SDI) systems for vibration control

Ruifu Zhang[1,2,*], **Jieling Jiang**[1,2], **Yingqi Jia**[1,2] **and Chao Wang**[1,2]

[1] State Key Laboratory of Disaster Reduction in Civil Engineering, Tongji University, Shanghai 200092, People's Republic of China
[2] Department of Disaster Mitigation for Structures, Tongji University, Shanghai 200092, People's Republic of China

E-mail: zhangruifu@tongji.edu.cn

Received 29 March 2021, revised 2 June 2021
Accepted for publication 14 June 2021
Published 30 June 2021

Abstract

A shape memory alloy damping inerter (SDI) with an SMA placed in parallel with an inerter and then in serial with a spring was developed as a vibration control device, where the inerter is utilized to amplify the deformation of SMA to improve the energy dissipation capacity. However, SDI can have other mechanical layouts when an SMA, an inerter and a spring are involved, which may exhibit different control effectiveness. Moreover, explicit design methods aiming to achieve the optimal performance of the SDI systems remain unexplored. In this study, SDIs with different mechanical layouts are proposed and compared, and design method for the SDI-equipped structure is developed. Firstly, the mechanical model of a structure with SDI systems is separately established. Parametric analysis is then conducted in terms of the displacement response, acceleration response and damping enhancement effect. Selection for appropriate SDI mechanical layout can be identified based on parametric analysis results. Additionally, design method based on maximizing the damping enhancement effect to fully develop the energy dissipation capacity of the SMA under the target structural response mitigation ratio is proposed. The performance of the optimal designed SDI-equipped structures is finally evaluated in the time-domain. Results show that both the displacement and acceleration responses of the SDI-equipped structures can be effectively mitigated by using the proposed optimal design method. Among the optimized SDI systems, the energy dissipation capacity of SMA is almost similar. Different SDI systems differ in the energy dissipation characteristic. The SMA-spring-paralleled SDI exhibits minimum damping force, indicating a better damping enhancement effect and less material demand of SMA than the other SDI systems.

Keywords: inerter, shape memory alloy, damper, damping enhancement effect

(Some figures may appear in color only in the online journal)

1. Introduction

Structural vibration control technologies have been proven to be an effective strategy to ensure structural safety under different external excitation [1–3]. The passive control technology is widely used owing to its long-term reliable control effect [4–6], and various passive dampers have been proposed and investigated [7–9]. The working principle of these dampers is to dissipate most of the energy transferred to the primary structure, thereby reducing the structural vibration responses. Shape memory alloy (SMA) known as a smart material with the unique super-elastic property is a promising energy dissipation material in structure control [10–12]. It can provide a stable hysteretic loop and energy dissipation capacity without permanent residual deformation [13, 14].

* Author to whom any correspondence should be addressed.

On top of that, a variety of SMA-based dampers have been proposed and investigated [15–17]. Mishra *et al* [18] combined the SMA with the tuned mass damper to reduce the mass ratio of the conventional tuned mass damper. Parulekar *et al* [19] analyzed a steel structure with an SMA damper and shake table tests were carried out to validate its control effectiveness. Silwal *et al* [17] proposed a super-elastic viscous damper that combined the re-centering capability of SMA and energy dissipation capability of the viscoelastic damper. Qian *et al* [20] experimentally investigated the performance of a re-centering SMA friction damper where the input energy was dissipated by the integrated friction devices. Qiu *et al* [21] developed an SMA-based self-centering damper which mainly utilized the re-centering capability of SMA. As summarized above, SMA-based devices are effective in mitigating vibration responses and reducing structural residual deformation. However, these devices mainly focused on directly utilizing the hysteretic characteristic of SMA to dissipate the vibration energy or the re-centering capability of SMA. Considering that the inherent damping of SMAs is limited, a large amount of SMAs are usually needed to achieve the desired energy dissipation effect, which may potentially bring high material demand [17]. Therefore, some researchers also combined SMAs with other geometrical amplification devices to further improve the energy dissipation capacity of SMA. Li *et al* [22] proposed a scissor-SMA damper with the displacement magnification characteristic, which achieved a larger response reduction compared to the devices without displacement magnification. Zhang *et al* [23] employed a level system to amplify the deformation of the SMA-friction damper and a ten-story frame building was adopted to validate its control effectiveness.

In addition to adopting the above methods to improve the energy dissipation capacity of SMA, inerter system with mass enhancement [8] and damping enhancement effects [24] also provides a potential alternative. Typical inerter systems comprise three basic mechanical elements: the inerter, the damping, and the spring elements [7, 25]. The inerter is a two-terminal mechanical element in which the resisting force is proportional to the relative accelerations between its two terminals [8, 26, 27]: $F_{\rm in} = m_{\rm in}(\ddot{u}_2 - \ddot{u}_1)$, where $m_{\rm in}$ is the inertance with a dimension of mass, $\ddot{u}_2$ and $\ddot{u}_1$ are the accelerations of its two terminals. The implementation of the two-terminal inertial element was initiated by Kawamata in 1973 [26]. At the beginning of this century, Saito *et al* [28] and Ikago *et al* [8, 29] proposed the tuned viscous mass damper, explicitly using the mass enhancement and damping enhancement effects of the inerter system. When the inerter element is excited by the external force, it can generate apparent mass (inertance) far greater than the gravitational mass of the inerter element, therefore more vibration energy can be absorbed without introducing extra inertia force to the primary structure [8]. Additionally, when the inerter element is serial connected to the spring element, the deformation of the damping element can be enhanced owing to the asynchronous vibration of the inerter system, thereby the damping element can dissipate more energy, which is the damping enhancement effect of the inerter system [8, 24]. Zhang *et al* [24] discovered and proved the damping enhancement equation which revealed the theoretical essence of the damping enhancement effect. Based on the damping enhancement effect of the inerter system, Jia *et al* [30] developed an innovative SMA damping inerter (SDI) and demonstrated its effectiveness in mitigating structural seismic responses, where the inerter element was in parallel with the SMA and then serially connected to a spring element. And the parameters of the proposed SDI were determined by approximate estimation. After SDI was proposed [30], other scholars have also begun to work on SDI system. Das *et al* [31] proposed an SDI system for wind-induced vibration control, where the SMA is in parallel with an electromagnetic transducer for energy harvesting purposes. Tiwari *et al* [32] combined the SDI system with the tuned mass to control the vibration response of the adjacent system, where the SMA, the tuned mass and the inerter are within a serial layout. Additionally, when only three basic mechanical elements (an SMA, a spring and an inerter) are involved within the SDI, it can have other mechanical layouts which may exhibit different control effectiveness. And an explicit optimal design method applicable to the SDI-equipped structure remains unexplored. Therefore, it is necessary to identify the characteristic of different mechanical layouts of SDI, and on this basis propose an optimal design method to optimize the parameters of SDI systems.

In this study, SDI systems with different layouts of the three basic mechanical elements are proposed and compared, and a design method applicable to the SDI-equipped structure is developed. To this end, the structure with different SDI systems is separately established. The governing equations of motion of each SDI-equipped structure are respectively given, and random vibration analysis is carried out based on the equivalent linearization of the nonlinear SMA in section 2. An extensive parametric analysis concerning the key parameters of the SDI is then conducted in section 3 in terms of the displacement response, acceleration response and damping enhancement effect. Subsequently in section 4, under target displacement and acceleration response mitigation ratio, an optimal design method aiming to maximize the damping enhancement effect of the SDI systems to fully develop the energy dissipation capacity of the SMA is proposed. Different target structural response mitigation ratios are considered as the design cases, the performance of the optimal designed SDI-equipped structures is finally evaluated in the time domain. Eventually, conclusions are drawn in section 5.

2. Theoretical analysis of structure equipped with the SDI system

2.1. Mechanical model

As depicted in figure 1, for the three basic mechanical elements within the SDI, the damping enhancement effect of the SDI can be generated when the inerter element is serially connected to the spring element owing to the asynchronous vibration between the serial inerter and spring element [8, 24, 33]. In other words, the deformation of the SMA in SDI can be amplified by the inner actions between the inerter

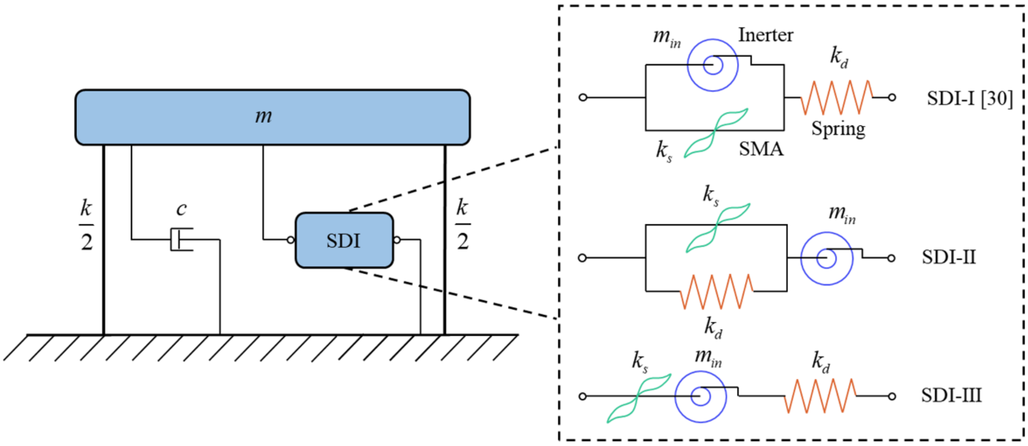

Figure 1. Schematics of the SDOF structure equipped with SDI system.

element and the serial spring element. Because of this damping enhancement mechanism, the SMA in the SDI can dissipate more vibration energy than a pure SMA damper [30]. Therefore, three basic layouts of an inerter element with inertance m_{in}, an SMA with initial stiffness k_{s}, and a spring element with stiffness k_{d} are considered and labeled as SDI-I [30], SDI-II and SDI-III, respectively. The 1st one is SDI-I [30], where the inerter element is placed in parallel to the SMA, and then serially connected to the spring; in the 2nd layout (referred to as SDI-II), the SMA is placed in parallel to the spring and then in series with the inerter; in the 3rd layout (denoted as SDI-III), all three elements are serial connected. A single-degree-of-freedom (SDOF) structure with a mass element (m), a spring element (k), and a damping element (c) equipped with an SDI system is adopted as the analytical model. The governing equations of motion are established based on the dynamic equilibrium condition, respectively. For the SDI-I equipped structure [30]:

$$\begin{cases} m\ddot{u} + c\dot{u} + ku + k_{\text{d}}(u - u_{\text{in}}) = -ma_g \\ m_{\text{in}}\ddot{u}_{\text{in}} + F_{\text{SMA}} = k_{\text{d}}(u - u_{\text{in}}) \end{cases}. \tag{1}$$

For the SDI-II equipped structure:

$$\begin{cases} m\ddot{u} + c\dot{u} + ku + m_{\text{in}}\ddot{u}_{\text{in}} = -ma_{\text{g}} \\ k_{\text{d}}(u - u_{\text{in}}) + F_{\text{SMA}} = m_{\text{in}}\ddot{u}_{\text{in}} \end{cases}. \tag{2}$$

For the SDI-III equipped structure:

$$\begin{cases} m\ddot{u} + c\dot{u} + ku + m_{\text{in}}\ddot{u}_{\text{in}} = -ma_{\text{g}} \\ k_{\text{d}}(u - u_{\text{in}} - u_{\text{s}}) = m_{\text{in}}\ddot{u}_{\text{in}} = F_{\text{SMA}} \end{cases}. \tag{3}$$

in which u, u_{in} and u_{s} represent the relative displacements of the structure, the inerter element and the SMA, respectively; a_{g} is the ground acceleration; F_{SMA} is the restoring force of the SMA which can be expressed as [18, 34]:

$$F_{\text{SMA}} = \alpha k_{\text{s}} u_{\text{s}} + (1 - \alpha) k_{\text{s}} Z_{\text{s}} \tag{4}$$

where α represents the stiffness ratio of SMA's stiffness in martensite phase to austenite phase [18, 34]; k_{s} is the initial stiffness of SMA in austenite phase; Z_{s} represents the hysteretic component of displacement in the SMA, which is the function of the displacement u_{s} [34]:

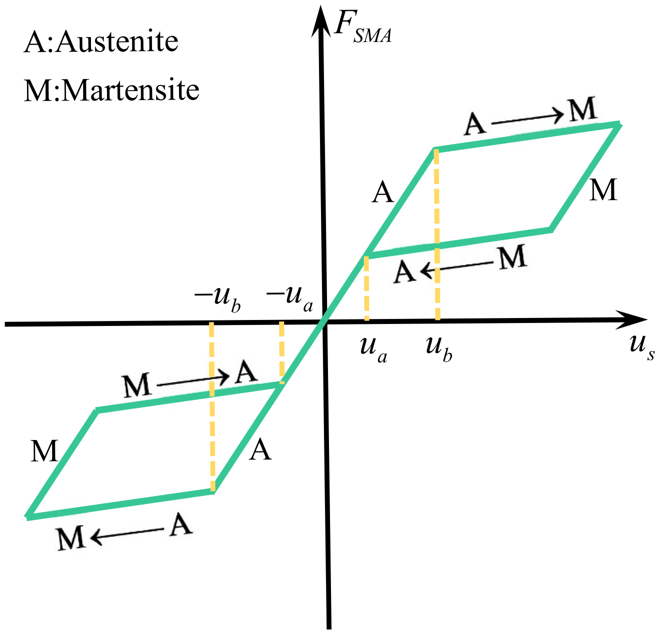

Figure 2. Force–deformation relationship of the super-elastic SMA.

$$\begin{aligned} Z_{\text{s}} = &\{1 - \text{sign}[\text{sign}(|u_{\text{s}}| - u_{\text{a}}) + 1]\} u_{\text{s}} \\ &+ \frac{\text{sign}(|u_{\text{s}}| - u_{\text{a}}) + 1}{2} \left[\frac{\text{sign}(u_{\text{s}}) + \text{sign}(\dot{u}_{\text{s}})}{2} (u_{\text{b}} - u_{\text{a}}) \right. \\ &\left. + u_{\text{a}} \,\text{sign}(u_{\text{s}}) \right] \end{aligned} \tag{5}$$

in which sign(u_{s}) is a sign function gives -1, 0 or 1 depending on u_{s} is negative, zero or positive; u_{a} and u_{b} are the elastic limits of austenite phase and the displacement triggering martensite phase transition, respectively. The detailed force–deformation relationship of the super-elastic SMA can therefore be shown in figure 2.

2.2. Stochastic response solutions

From the above section, it can be seen in figure 2 that the force-deformation relationship of SMA exhibits nonlinear behavior. In the mathematical modeling of the nonlinear behavior of the SMA [34–37], the stochastic equivalent linearization method is widely used [34, 36] to derive the stochastic responses under random excitations, which enables the nonlinear term Z_s in equation (4) replaced by the equivalent linearized form $\tilde{Z}_s$ as follows [34]:

$$\tilde{Z}_s = \tilde{c}\dot{u}_s + \tilde{k}u_s \tag{6}$$

where $\tilde{c}$ and $\tilde{k}$ are the equivalent linearized coefficient, determined by minimizing the mean square error between the actual nonlinear model Z_s and the equivalent linearized model $\tilde{Z}_s$, that is:

$$\frac{\partial\left[E\left(\tilde{Z}_s - Z_s\right)^2\right]}{\partial\tilde{c}} = 0, \frac{\partial\left[E\left(\tilde{Z}_s - Z_s\right)^2\right]}{\partial\tilde{k}} = 0 \tag{7}$$

in which $E[]$ represents the expectation operator. Solving equation (7) yields that:

$$\tilde{c} = \frac{E[\dot{u}_s \cdot Z_s]}{E[\dot{u}_s^2]}, \tilde{k} = \frac{E[u_s \cdot Z_s]}{E[u_s^2]} \tag{8}$$

Substituting equation (5) into equation (8) follows that [34]:

$$\tilde{c} = \frac{(u_b - u_a)}{\sqrt{2\pi}\sigma_{\dot{u}_s}}\left[1 - \mathrm{erf}\left(\frac{u_a}{\sqrt{2}\sigma_{u_s}}\right)\right], \tilde{k} = \frac{(u_a + u_b)}{\sqrt{2\pi}\sigma_{u_s}}\exp\left(\frac{-u_a^2}{2\sigma_{u_s}^2}\right) \tag{9}$$

in which σ_{u_s} and $\sigma_{\dot{u}_s}$ are the root-mean-square values of u_s and $\dot{u}_s$, respectively, and $\mathrm{erf}(\eta)$ is the error function expressed as:

$$\mathrm{erf}(\eta) = \frac{2}{\sqrt{\pi}}\int_0^\eta \mathrm{e}^{-\chi^2}\mathrm{d}\chi. \tag{10}$$

Substituting equation (6) into equation (4), the equivalent form of the restoring force of the SMA can be obtained.

$$F_{\mathrm{SMA}} = \alpha k_s u_s + (1-\alpha)k_s\left(\tilde{c}\dot{u}_s + \tilde{k}u_s\right) = c_{\mathrm{eq}}\dot{u}_s + k_{\mathrm{eq}}u_s \tag{11}$$

where the equivalent stiffness k_{eq} and the equivalent damping coefficient c_{eq} in equation (11) can then be expressed as:

$$\begin{cases} c_{\mathrm{eq}} = (1-\alpha)k_s\tilde{c} \\ k_{\mathrm{eq}} = \alpha k_s + (1-\alpha)k_s\tilde{k} \end{cases}. \tag{12}$$

Once the restoring force F_{SMA} is linearized through the equivalent linearization method, the equations (1)–(3) can be all expressed in the matrix form as follows:

$$\mathbf{M}\ddot{\mathbf{u}} + \mathbf{C}\dot{\mathbf{u}} + \mathbf{K}\mathbf{u} = -\boldsymbol{M\tau}a_g \tag{13}$$

where $\mathbf{M}$, $\mathbf{C}$ and $\mathbf{K}$ represent the mass, damping and stiffness matrices, respectively; $\mathbf{u}$, $\dot{\mathbf{u}}$ and $\ddot{\mathbf{u}}$ are the vectors of displacement, velocity, and acceleration relative to the ground, respectively; $\boldsymbol{\tau}$ is the load influence vector.

Owing to different mechanical layouts of the three elements, the mass, damping, and stiffness matrices in equation (13) differ. For the SDI-I equipped structure, the matrices and vectors entering equation (13) can be expressed as [30]:

$$\begin{aligned} &\mathbf{M} = \begin{bmatrix} m & \\ & m_{\mathrm{in}} \end{bmatrix}, \mathbf{C} = \begin{bmatrix} c & \\ & c_{\mathrm{eq}} \end{bmatrix}, \\ &\mathbf{K} = \begin{bmatrix} k + k_d & -k_d \\ -k_d & k_d + k_{\mathrm{eq}} \end{bmatrix}, \\ &\mathbf{u} = \begin{Bmatrix} u & u_{\mathrm{in}} \end{Bmatrix}^{\mathrm{T}}, \dot{\mathbf{u}} = \begin{Bmatrix} \dot{u} & \dot{u}_{\mathrm{in}} \end{Bmatrix}^{\mathrm{T}}, \\ &\ddot{\mathbf{u}} = \begin{Bmatrix} \ddot{u} & \ddot{u}_{\mathrm{in}} \end{Bmatrix}^{\mathrm{T}}, \boldsymbol{\tau} = \begin{Bmatrix} 1 & 0 \end{Bmatrix}^{\mathrm{T}}. \end{aligned} \tag{14}$$

Likewise, corresponding matrices for the SDI-II equipped structure take the following form:

$$\begin{aligned} &\mathbf{M} = \begin{bmatrix} m & \\ & m_{\mathrm{in}} \end{bmatrix}, \mathbf{C} = \begin{bmatrix} c + c_{\mathrm{eq}} & -c_{\mathrm{eq}} \\ -c_{\mathrm{eq}} & c_{\mathrm{eq}} \end{bmatrix}, \\ &\mathbf{K} = \begin{bmatrix} k + k_d + k_{\mathrm{eq}} & -(k_d + k_{\mathrm{eq}}) \\ -(k_d + k_{\mathrm{eq}}) & k_d + k_{\mathrm{eq}} \end{bmatrix}, \mathbf{u} = \begin{Bmatrix} u & u_{\mathrm{in}} \end{Bmatrix}^{\mathrm{T}}, \\ &\dot{\mathbf{u}} = \begin{Bmatrix} \dot{u} & \dot{u}_{\mathrm{in}} \end{Bmatrix}^{\mathrm{T}}, \ddot{\mathbf{u}} = \begin{Bmatrix} \ddot{u} & \ddot{u}_{\mathrm{in}} \end{Bmatrix}^{\mathrm{T}}, \boldsymbol{\tau} = \begin{Bmatrix} 1 & 0 \end{Bmatrix}^{\mathrm{T}}. \end{aligned} \tag{15}$$

Similarly, the matrix forms for the SDI-III equipped structure can be expressed as follows:

$$\begin{aligned} &\mathbf{M} = \begin{bmatrix} m & & \\ & m_{\mathrm{in}} & \\ & & 0 \end{bmatrix}, \mathbf{C} = \begin{bmatrix} c & & \\ & 0 & \\ & & c_{\mathrm{eq}} \end{bmatrix}, \\ &\mathbf{K} = \begin{bmatrix} k + k_d & -k_d & -k_d \\ -k_d & k_d & k_d \\ -k_d & k_d & k_d + k_{\mathrm{eq}} \end{bmatrix}, \mathbf{u} = \begin{Bmatrix} u & u_{\mathrm{in}} & u_s \end{Bmatrix}^{\mathrm{T}}, \\ &\dot{\mathbf{u}} = \begin{Bmatrix} \dot{u} & \dot{u}_{\mathrm{in}} & \dot{u}_s \end{Bmatrix}^{\mathrm{T}}, \ddot{\mathbf{u}} = \begin{Bmatrix} \ddot{u} & \ddot{u}_{\mathrm{in}} & \ddot{u}_s \end{Bmatrix}^{\mathrm{T}}, \\ &\boldsymbol{\tau} = \begin{Bmatrix} 1 & 0 & 0 \end{Bmatrix}^{\mathrm{T}}. \end{aligned} \tag{16}$$

Then equation (13) can be formulated into the space-state forms as follows:

$$\begin{bmatrix} \mathbf{O} & \mathbf{M} \\ \mathbf{M} & \mathbf{C} \end{bmatrix}\begin{Bmatrix} \ddot{\mathbf{u}} \\ \dot{\mathbf{u}} \end{Bmatrix} + \begin{bmatrix} -\mathbf{M} & \mathbf{O} \\ \mathbf{O} & \mathbf{C} \end{bmatrix}\begin{Bmatrix} \dot{\mathbf{u}} \\ \mathbf{u} \end{Bmatrix} = \begin{Bmatrix} \mathbf{0} \\ -\boldsymbol{M\tau} \end{Bmatrix} a_g \tag{17}$$

where O and $\mathbf{0}$ denote the zero matrix and zero vector, respectively.

Considering the stochastic feature of the vibration process, random vibration analysis is adopted to obtain the mean-square responses of the SDI-equipped structure. The pseudo excitation method [38–40] is used to obtain the power spectral density of structural dynamic response, which is an efficient and accurate method to solve the governing equations of motion under random excitation. Assuming the ground acceleration a_g in equation (13) is harmonic which can be expressed as:

$$a_g = \sqrt{S_g(\omega)}\mathrm{e}^{i\omega t} \tag{18}$$

where $S_g(\omega)$ is the input power spectral density. The calculated response in equation (17) can then take the following form:

$$\mathbf{u}(t) = \mathbf{u}(\omega)\mathrm{e}^{i\omega t}. \tag{19}$$

Substituting equation (19) into equation (17), the power spectral density of the structural response can be calculated as follows:

$$\mathbf{S_u}(\omega) = \bar{\mathbf{u}}(\omega) \odot \mathbf{u}(\omega) \tag{20}$$

where $\bar{\mathbf{u}}$ represents the conjugate matrix of the relative displacement response vector $\mathbf{u}$, and the symbol $\odot$ denotes the Hadamard product calculation.

The variance for structural displacement can subsequently be calculated as:

$$\sigma_{\mathrm{u}}^2 = \int_{-\infty}^{\infty} S_{\mathrm{u}}(\omega)\,\mathrm{d}\omega. \tag{21}$$

Similarly, the variance for absolute acceleration response can be obtained:

$$\sigma_{\mathrm{a}}^2 = \int_{-\infty}^{\infty} S_{\mathrm{a}}(\omega)\,\mathrm{d}\omega. \tag{22}$$

Considering the stochastic nature of the ground acceleration, the input power spectral density function applied in equation (18) is modeled using the Kanai–Tajimi filtered spectrum modified by Clough and Penzien [41], with the 2nd filter in series based on the Kanai–Tajimi spectrum. The Clough and Penzien spectrum makes $S_{a_g}(\omega)$ tends to be zero as ω approaches to zero, avoiding the unrealistically high values of the power spectral density in a low-frequency area. Therefore, the Clough and Penzien spectrum is more realistic to the actual ground excitation process and has wider applicability, which can be expressed as follows [42, 43]:

$$S_{a_g}(\omega) = S_0 \frac{\omega_g^4 + 4\zeta_g^2\omega_g^2\omega^2}{\left(\omega_g^2 - \omega^2\right)^2 + 4\zeta_g^2\omega_g^2\omega^2} \frac{\omega^4}{\left(\omega_f^2 - \omega^2\right)^2 + 4\zeta_f^2\omega_f^2\omega^2} \tag{23}$$

where $S_{a_g}(\omega)$ is the filtered power spectral density; ω is the filter frequency; S_0 is the spectral density of the white noise excitation; ω_g and ζ_g are the natural frequency and damping ratio of the soil characteristic, respectively; ω_f and ζ_f denote the fundamental frequency and the equivalent damping ratio of the soil filter, respectively. Considering the characteristic of the soil is not the primary concern of this study and for further study in the subsequent section, parameters ω_g, ζ_g, ω_f and ζ_f are taken as $\omega_g = 12.5\,\mathrm{rad\,s^{-1}}$, $\zeta_g = 0.6$, $\omega_f = 2\,\mathrm{rad\,s^{-1}}$ and $\zeta_f = 0.7$ according to the literature [44, 45].

3. Parametric analysis

To facilitate the comparison among the SDI systems, parametric studies concerning the key parameters of the SDI are carried out in this section. A 2% damping SDOF structure with a mass of 20 000 kg and natural period 0.54 s is adopted as the analytical model [46]. Considering the intrinsic property of SMA is not the main concern of this study, the relevant parameters of SMA are first assumed for $\alpha = 0.1$, $u_a = 0.005\,\mathrm{m}$ and $u_b = 0.05\,\mathrm{m}$ according to the literature [18].

3.1. Performance indices

Three dimensionless indicators are pre-defined here to normalize the parameters of SDI.

$$\mu = m_{\mathrm{in}}/m, \quad \lambda = k_s/k, \quad \kappa = k_d/k \tag{24}$$

where μ is the inertance-mass ratio; λ is the stiffness ratio of the SMA concerning the primary structure; κ is the stiffness ratio of the spring element to the primary structure. In addition, the performance indices are defined:

$$\gamma_{\mathrm{u}} = \frac{\sigma_{\mathrm{u,SDI}}}{\sigma_{\mathrm{u,0}}}, \gamma_{\mathrm{a}} = \frac{\sigma_{\mathrm{a,SDI}}}{\sigma_{\mathrm{a,0}}}, \gamma_{\mathrm{d}} = \frac{\sigma_{\mathrm{u,SMA}}}{\sigma_{\mathrm{u}}} \tag{25}$$

where γ_u, γ_a and γ_d are the displacement response mitigation ratio, acceleration response mitigation ratio and damping deformation enhancement ratio, respectively. γ_u or γ_a smaller than one indicates that the equipped SDI is effective in reducing the displacement or acceleration responses. Owing to the asynchronous vibration within the inerter system, the deformation of the SMA within the SDI systems can be magnified [24]. Therefore, γ_d is defined as an energy dissipation evaluation indicator of the SDI, which reflects the damping enhancement efficiency of the SDI. A larger γ_d implies that the deformation of the SMA is more effectively magnified and more vibration energy can be dissipated. Therefore, the damping enhancement effect of the SDI can be fully utilized and the energy dissipation capacity of the SMA meanwhile can be fully developed.

3.2. Structural response mitigation effect

Parameters analyses are conducted for different values of μ (0.05, 0.1 and 0.2) with λ and κ varying continuously in the range of $10^{-2} - 10^{0}$, noted that the selection of μ and a similar range of λ and κ was investigated in the previous relevant study [7, 25]. The contour plots of γ_u are shown in figures 3, 5 and 7, with a specific color within the parameter space representing the numerical value of γ_u. During the analysis process, it is observed that the shape and variation trend of the figures of γ_a are similar to that of γ_u, as shown in figures 4, 6 and 8.

It can be seen from figure 3 that with the increase of μ, the minimum value of γ_u in each subplot decreases, and the desired value of λ and κ for a decrease in γ_u shift to the upper bound of the parameter ranges. When μ is determined, a lower value of γ_u is generally accompanied by increases in

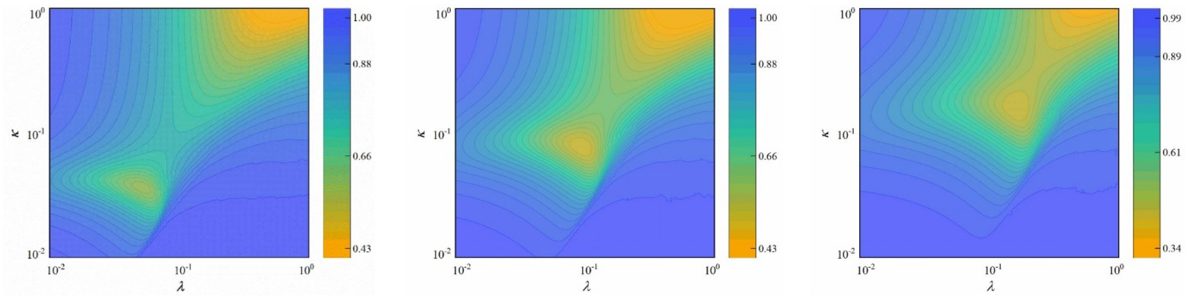

(a) $\mu = 0.05$ (b) $\mu = 0.1$ (c) $\mu = 0.2$

Figure 3. Comparison of γ_u under different μ for the SDI-I equipped structure.

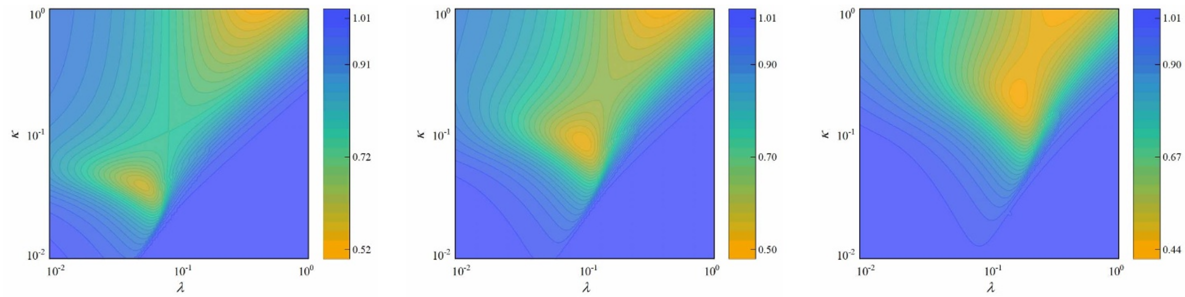

(a) $\mu = 0.05$ (b) $\mu = 0.1$ (c) $\mu = 0.2$

Figure 4. Comparison of γ_a under different μ for the SDI-I equipped structure.

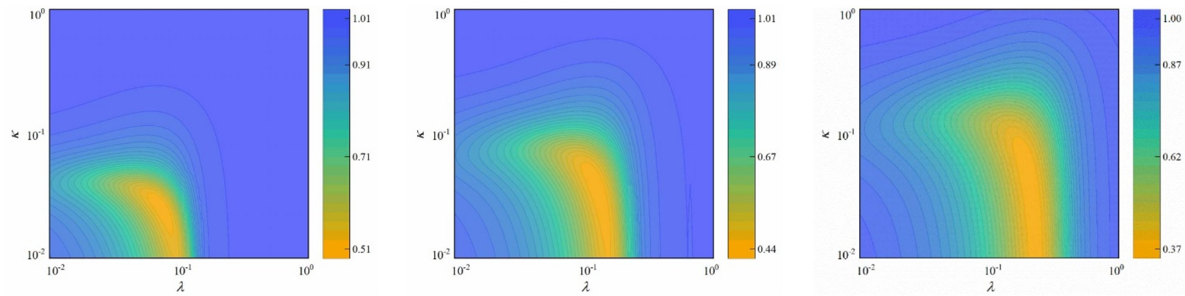

(a) $\mu = 0.05$ (b) $\mu = 0.1$ (c) $\mu = 0.2$

Figure 5. Comparison of γ_u under different μ for the SDI-II equipped structure.

λ and κ. Additionally, closed contour lines can be observed when μ is fixed, which implies that the optimal solution for minimum γ_u can be obtained within the closed contour areas. Compared with γ_u, the minimum value of γ_a is slightly larger than γ_u when μ is fixed, which indicates that SDI-I can reduce the displacement and acceleration responses simultaneously while the efficiency in controlling the displacement response is higher than the latter.

In the condition of the same parameter range of μ, λ and κ, the contour plots of the SDI-II equipped structure are also provided in figures 5 and 6. Different from the SDI-I system, the location of the minimum γ_u appears at a lower value of κ, which signifies that the SDI-II is more effective in response mitigation (both displacement and acceleration response) when κ takes a smaller value (when the stiffness of the support is small). And an increase in μ leads to a broader region of the small value of γ_u and γ_a. With fixed μ, the effective response mitigation area locates at the inner part of the parametric space with each contour plot has a peak point, in other words, the reasonable parameter sets of SDI-II (μ, λ and κ) can be optimized within the parameter interval. Meanwhile, from figure 5 it can be seen that the variation trends of γ_a are similar to γ_u. But the boundaries of the contour lines are broader and more diffused when γ_a is relatively larger (the dark blue area).

Concerning SDI-III equipped structure, a different variation pattern of γ_u and γ_a can be observed, where the contour plot forms a valley instead of a peak. An increase in μ leads to

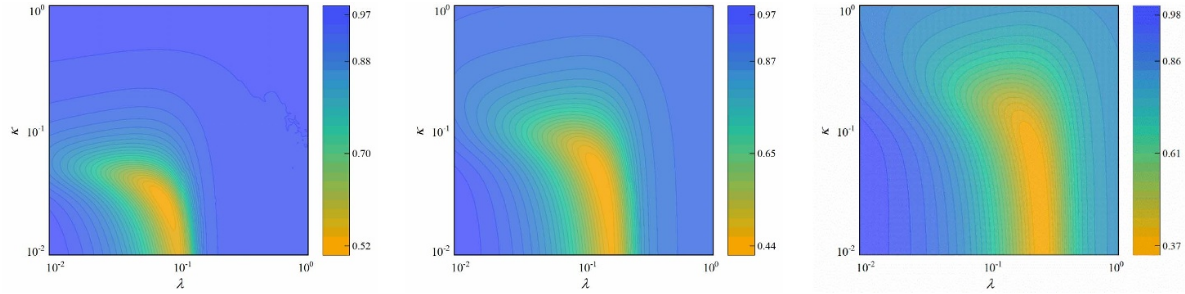

(a) $\mu = 0.05$ (b) $\mu = 0.1$ (c) $\mu = 0.2$

Figure 6. Comparison of γ_a under different μ for the SDI-II equipped structure.

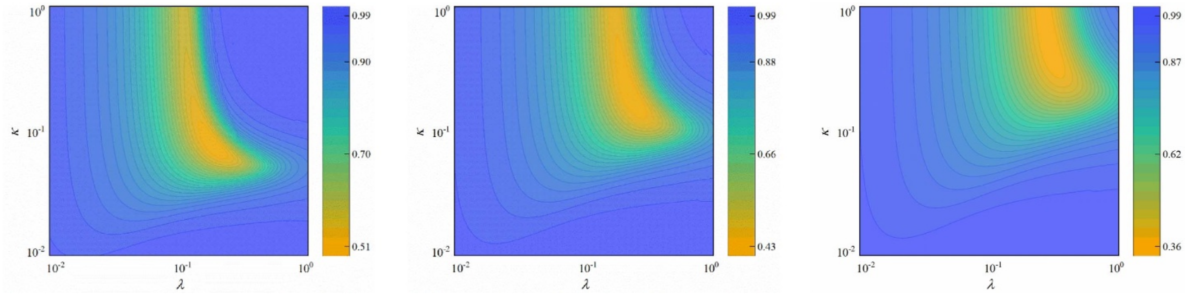

(a) $\mu = 0.05$ (b) $\mu = 0.1$ (c) $\mu = 0.2$

Figure 7. Comparison of γ_u under different μ for the SDI-III equipped structure.

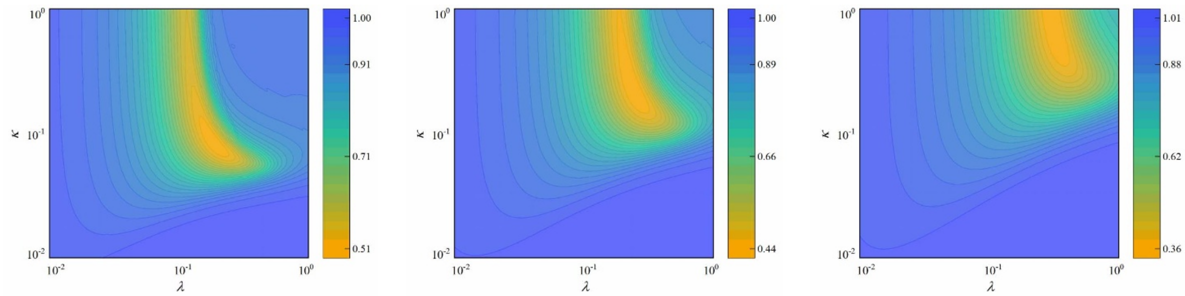

(a) $\mu = 0.05$ (b) $\mu = 0.1$ (c) $\mu = 0.2$

Figure 8. Comparison of γ_a under different μ for the SDI-III equipped structure.

a smaller value of γ_u and γ_a. Additionally, different from the SDI-II controlled case, SDI-III is more effective in reducing the response (both displacement and acceleration response) when κ takes a larger value (when the stiffness of the support is large).

3.3. Damping enhancement effect

Values of γ_d, similarly, can be calculated for the SDI-equipped structure, and the contour plots are depicted in figures 9–11. From the trend of γ_d shown in figure 9, with the increase of μ, the peak value of γ_d decreases, which indicates that the increase in μ can lower the damping enhancement effect of the SDI-I. And the peak location of the contour plots moves along the positive direction of λ axis and κ axis. When μ is determined, the larger γ_d is accompanied by a relatively wide range of λ and a designated area of κ (blue area). As regards the SDI-II controlled case, an increase in μ can lead to a broader region of the larger value of γ_d with a peak decrease in γ_d, which is similar to the SDI-I controlled situation. However, the peak value of γ_d with the same μ is slightly larger than the SDI-I controlled case. When the three elements are both connected in series (SDI-III), similar to the above two discussed cases, γ_d decreases with the increase of μ. A larger γ_d is accompanied with a larger λ and κ when μ is fixed. Comparing SDI-I and SDI-II controlled cases, it is noticeable that the peak value of γ_d in the SDI-III equipped structure is smaller which implies the damping enhancement effect of SDI-III is relatively small among the SDI systems.

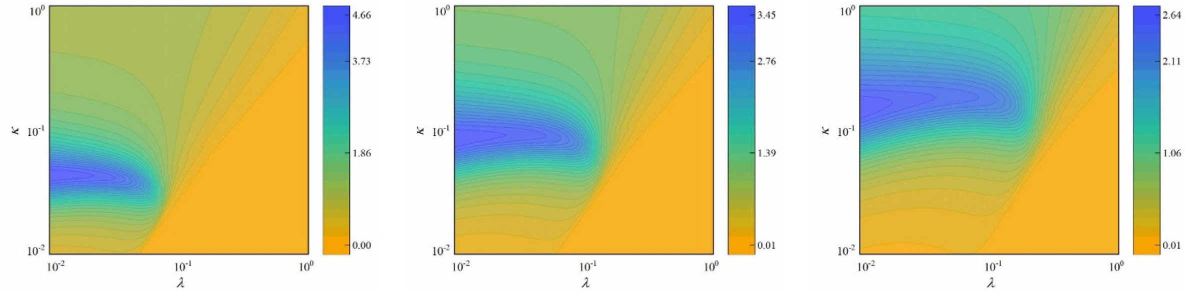

(a) $\mu = 0.05$ (b) $\mu = 0.1$ (c) $\mu = 0.2$

Figure 9. Comparison of γ_d under different μ for the SDI-I equipped structure.

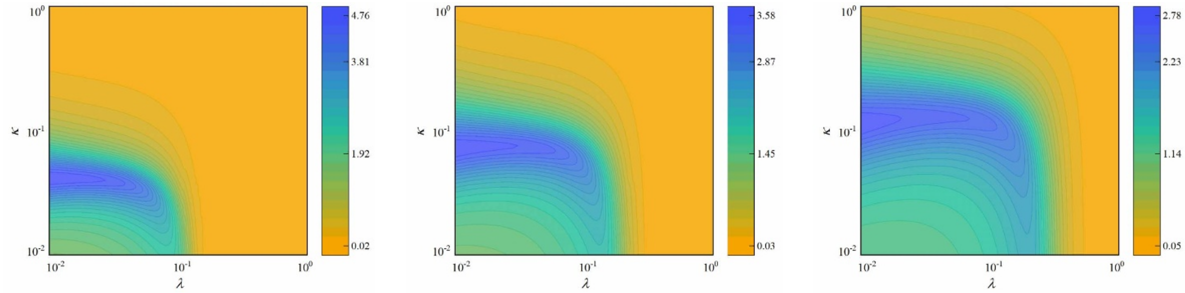

(a) $\mu = 0.05$ (b) $\mu = 0.1$ (c) $\mu = 0.2$

Figure 10. Comparison of γ_d under different μ for the SDI-II equipped structure.

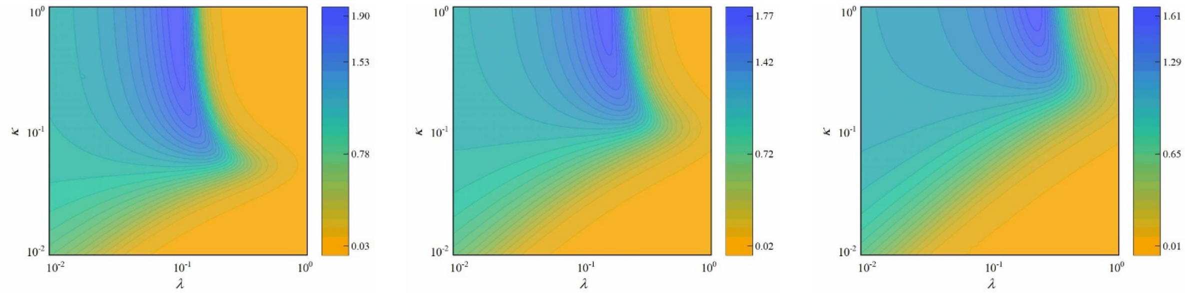

(a) $\mu = 0.05$ (b) $\mu = 0.1$ (c) $\mu = 0.2$

Figure 11. Comparison of γ_d under different μ for the SDI-III equipped structure.

4. Parameter optimization of SDI system

4.1. Optimal design method

As discussed in the above parametric analysis, it can be observed that different mechanical layouts of the SMA, spring, and inerter elements lead to a different control characteristic even though the input parameters are the same. Moreover, the effective parameter sets (μ, λ and κ) for effective response mitigation need to be acquired optimally since not all parameter leads to a beneficial response control. Therefore, the goal in this section is to develop an optimal design method for determining the parameters of SDI systems. During the design process, both the structural response mitigation effect and the damping enhancement effect are desirable to be achieved, in other words, γ_u or γ_a is expected to be as small as possible to achieve effective response mitigation effect and γ_d is expected to be larger to fully utilize the beneficial damping enhancement effect of the SDI. From section 3 it can be observed that the optimal area of these two effects exists some deviations. To achieve the optimal balance between the structural response mitigation and the damping enhancement effect, γ_d is considered as the objective function for optimization which reflects the degree of the damping enhancement effect of the SDI. The target displacement response mitigation ratio $\gamma_{u,t}$ and the target acceleration response mitigation ratio $\gamma_{a,t}$ which reflect the performance of the SDI-equipped structure construct the constraint condition. Consequently, the design process aims to find the optimal parameter set (μ, λ and κ) that generates the maximum value of γ_d under the pre-specified

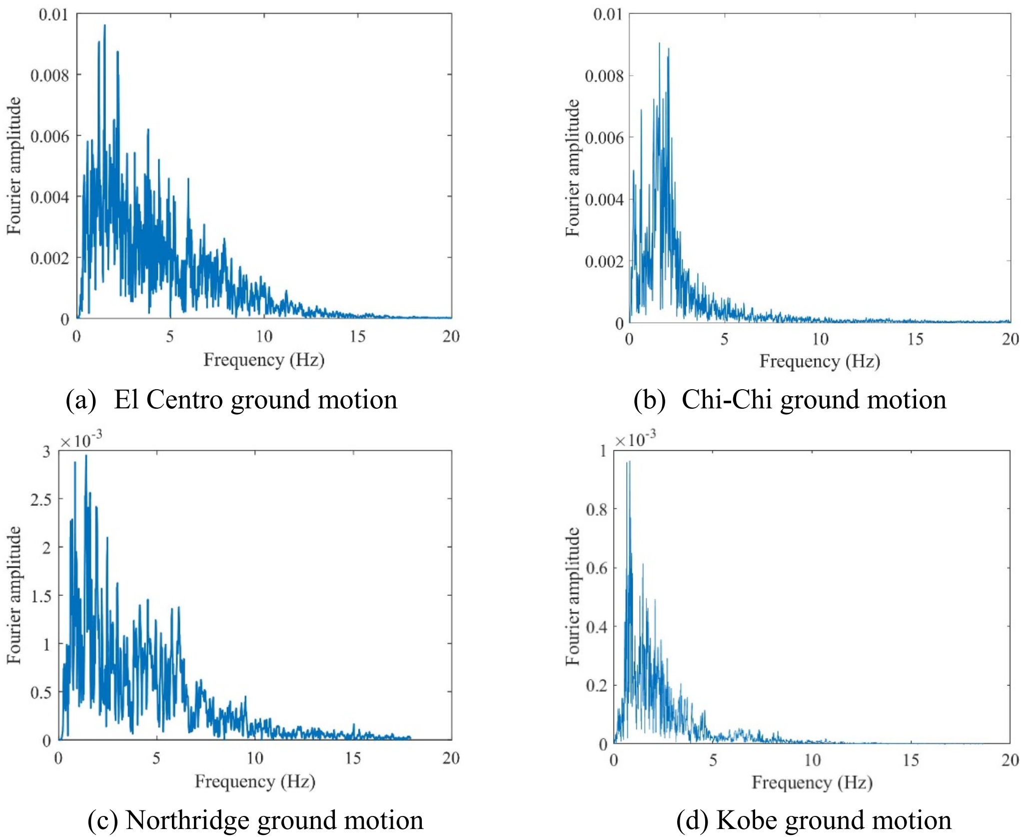

Figure 12. Fourier amplitude spectrum of four natural ground motions.

$\gamma_{u,t}$ and $\gamma_{a,t}$. Based on the above discussion, the optimization problem can be expressed in mathematical form as follows:

$$\begin{cases} \underset{\mu,\lambda \text{ and } \kappa}{\text{maximize}} & \gamma_d \\ \text{subject to} & \begin{cases} \gamma_u \leqslant \gamma_{u,t} \\ \gamma_a \leqslant \gamma_{a,t} \\ 0 < \mu \leqslant 1 \\ 0 < \lambda \leqslant 1 \\ 0 < \kappa \leqslant 1 \end{cases} \end{cases} \tag{26}$$

where $\gamma_{u,t}$ and $\gamma_{a,t}$ denote the target displacement response mitigation ratio and the target acceleration response mitigation ratio, respectively, which are determined based on the initial analysis of the structure. A computer program using the simulated annealing algorithm is developed to solve equation (26) in MATLAB [47] to obtain the optimal parameters of the SDI systems. The simulated annealing algorithm [48] is a random search algorithm for solving the combinational optimization problem. By simulating the natural annealing process, the global optimal solution of the object function in the parameter space can be obtained. During the iterative search process, the introduction of the natural annealing mechanism can avoid the drawbacks of being trapped in the local optimal solution, and is beneficial to improve the reliability of obtaining the global optimal solution. Additionally, the simulated annealing algorithm has been used to optimize the parameters of the inerter system in the previous study [49]. During the optimal design process, the threshold of the optimal parameters ranges from 0.01 to 1 corresponding to the parameter analysis conducted in section 3. The whole optimization procedure can be summarized as the following three steps:

Step 1: Conduct the initial analysis of the structure to evaluate its performance. Based on the analysis results, specify the target response mitigation ratio $\gamma_{u,t}$ and $\gamma_{a,t}$.

Step 2: Substituting the obtained $\gamma_{u,t}$ and $\gamma_{a,t}$ into equation (26), establish the parameter optimization formulation of the SDI-equipped structure.

Step 3: Operate the developed parameter optimization program and obtain the optimal parameters of the SDI: μ, λ and κ.

Based on the above proposed optimal design method, the same model discussed in section 3 is adopted as the design case. To achieve different performance levels and for an overall comparison among the SDI systems, three target vibration mitigation ratios are adopted. The selection of the specific value of $\gamma_{u,t}$ and $\gamma_{a,t}$ should consider two aspects: the desirable response mitigation effect and being achievable in all SDI systems. On this basis, the initial value of the target displacement mitigation ratio $\gamma_{u,t}$ is selected according to the lower value of figures 3 (γ_u = 0.34), 5 (γ_u = 0.37), and 7 (γ_u = 0.36). Based on this, the approximate value is assumed as $\gamma_{u,t} = 0.4$. Similarly, the initial value of the target acceleration mitigation ratio $\gamma_{a,t}$ is selected according to the lower value of figures 4 ($\gamma_a = 0.44$), 6 ($\gamma_a = 0.37$), and 8 ($\gamma_a = 0.36$). Therefore, the approximate value is assumed as $\gamma_{a,t} = 0.4$. The increment of both $\gamma_{u,t}$ and $\gamma_{a,t}$ is assumed as 0.1. In addition, figures 3–8 show that the three SDI systems can approximately get the minimum value of $\gamma_{u,t}$ and $\gamma_{a,t}$ nearly at the same position. Therefore, the combination method of $\gamma_{u,t}$ and $\gamma_{a,t}$ is chosen to be a direct one-to-one correspondence.

4.2. Structural displacement and acceleration response

In the previous section, the parametric analysis of the SDI is conducted using the Clough and Penzien spectrum to model the input ground motion. However, real ground motion is a non-stationary random process and the frequency component is various in general. Therefore, the parameter optimization process illustrated in the above section is carried out through the power spectral density of the real input ground motions in this section. Four natural ground motions comprising different frequency components are selected from the Pacific Earthquake Engineering Research database [50]: El Centro ground motion (1940 Imperial Valley earthquake), Chi–Chi ground motion (1999 Chi–Chi earthquake), Northridge ground motion (1994 Northridge earthquake) and Kobe ground motion (1995 Kobe earthquake). The Fourier amplitude spectrum which reflects the frequency characteristic of the ground motion and the normalized acceleration spectrum are depicted in figures 12 and 13.

The root-mean-square response mitigation ratio $\gamma_{u,RMS}$ and $\gamma_{a,RMS}$ calculated in the time domain are summarized in table 1. It is worth mentioning that the 1st Arabic number of the 1st column in the table represents the corresponding optimal target $\gamma_{u,t}$, and the 2nd number represents the $\gamma_{a,t}$. As presented in table 1, the target value ($\gamma_{u,t}$ and $\gamma_{a,t}$) and the root-mean-square value ($\gamma_{u,RMS}$ and $\gamma_{a,RMS}$) match each other, validating that the optimized parameters obtained based on the power spectral density of the actual input ground motions are reliable. The optimal results of μ, λ and κ as well as the corresponding γ_d under four input ground motions are tabulated in tables 2–5. With given $\gamma_{u,t}$ and $\gamma_{a,t}$, the obtained μ of SDI-I is generally larger than that of the SDI-II and SDI-III, which implies a larger space is required in the building to allocate the SDI-I mass. Meanwhile, $\gamma_d > 1$ indicates that the deformation of SMA is effectively amplified by the damping enhancement effect of the SDI systems, among which it is noticeable that damping enhancement of the SDI-II outperforms the others. Therefore, the SDI-II indicates a better damping enhancement effect and less material demand of SMA than the other SDI systems.

Time history responses of the SDI-equipped structure for $\gamma_{u,t} = 0.6$ and $\gamma_{a,t} = 0.6$ concerning the relative displacement response and absolute acceleration response are shown in figures 14–17. The conclusions drawn below based on $\gamma_{u,t} = 0.6$ and $\gamma_{a,t} = 0.6$ also hold for other control cases ($\gamma_{u,t} = 0.4$ with $\gamma_{a,t} = 0.4$ and $\gamma_{u,t} = 0.5$ with $\gamma_{a,t} = 0.5$). From the inspection of the relative displacement time history responses, the consistent conclusion can be summarized that all the SDI controlled cases can achieve the response mitigation effect, demonstrating the control effectiveness of the SDI systems. The 2nd array subplots in figures 14–17 show that the absolute acceleration responses of both the SDI controlled case

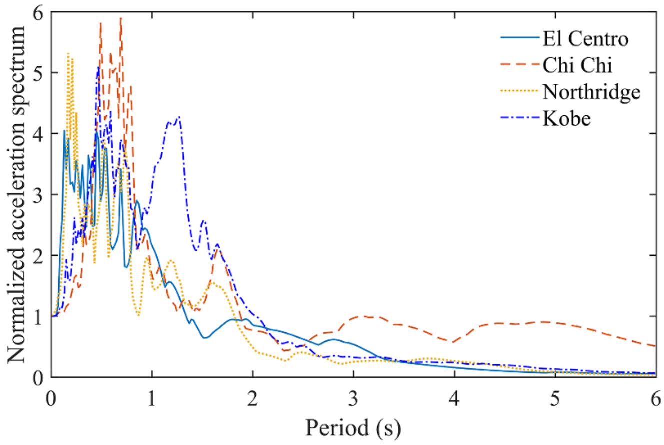

Figure 13. Normalized acceleration spectrum of four natural ground motions.

Table 1. Results of response mitigation ratio under control cases in section 4.1.

	$\gamma_{u,RMS}$ ($\gamma_{a,RMS}$)			
Control case	El Centro	Chi–Chi	Northridge	Kobe
SDI-I-0.4-0.4	0.39 (0.40)	0.40 (0.38)	0.40 (0.40)	0.40 (0.40)
SDI-II-0.4-0.4	0.39 (0.40)	0.40 (0.40)	0.40 (0.40)	0.40 (0.39)
SDI-III-0.4-0.4	0.39 (0.40)	0.40 (0.39)	0.40 (0.40)	0.40 (0.49)
SDI-I-0.5-0.5	0.49 (0.50)	0.49 (0.50)	0.50 (0.48)	0.50 (0.50)
SDI-II-0.5-0.5	0.49 (0.50)	0.49 (0.49)	0.50 (0.50)	0.50 (0.50)
SDI-III-0.5-0.5	0.48 (0.50)	0.49 (0.49)	0.49 (0.49)	0.50 (0.48)
SDI-I-0.6-0.6	0.60 (0.60)	0.59 (0.58)	0.60 (0.59)	0.60 (0.60)
SDI-II-0.6-0.6	0.58 (0.60)	0.60 (0.59)	0.59 (0.57)	0.60 (0.60)
SDI-III-0.6-0.6	0.57 (0.59)	0.60 (0.60)	0.60 (0.59)	0.60 (0.58)

are reduced simultaneously compared to the uncontrolled structure, which is consistent with the above parameter analysis results obtained in section 3.2.

4.3. Energy dissipation effect

For further comparison of the energy dissipation difference among the SDI-equipped structures, the energy dissipation ratio is defined here to evaluate the energy dissipation capacity of the SDI systems:

$$\gamma_E = \frac{E_{d,SDI}}{E_{input}} \tag{27}$$

where $E_{d,SDI}$ and E_{input} denote the energy dissipated by the SMA in the SDI and the total input structural energy, respectively. Larger γ_E indicates that the input energy is more dissipated effectively by the SDI. The energy dissipation ratio γ_E of both the SDI-controlled cases under different ground motions are tabulated in table 6. It is noticeable that over 60% of the input energy is effectively dissipated by the SDI systems under all controlled cases, indicating that less energy is transferred to the structure. And smaller $\gamma_{u,t}$ and $\gamma_{a,t}$ are accompanied by a larger portion of energy dissipation by the SDI systems. For

Table 2. Optimization results for SDI-equipped structure under El Centro ground motion.

Control case	Optimization results			
	μ	λ	κ	γ_d
SDI-I-0.4-0.4	0.4014	0.0764	0.5119	1.4796
SDI-II-0.4-0.4	0.2717	0.0729	0.1279	1.9979
SDI-III-0.4-0.4	0.2123	0.1306	0.5168	1.3833
SDI-I-0.5-0.5	0.1421	0.0246	0.1481	2.5713
SDI-II-0.5-0.5	0.0956	0.0344	0.0581	2.6843
SDI-III-0.5-0.5	0.1016	0.0604	0.7830	1.7191
SDI-I-0.6-0.6	0.0773	0.0152	0.0861	3.3936
SDI-II-0.6-0.6	0.0274	0.0102	0.0227	5.2529
SDI-III-0.6-0.6	0.0578	0.0391	0.9880	1.7747

Table 3. Optimization results for SDI-equipped structure under Chi–Chi ground motion.

Control case	Optimization results			
	μ	λ	κ	γ_d
SDI-I-0.4-0.4	0.4102	0.0690	0.3562	1.9933
SDI-II-0.4-0.4	0.2143	0.0652	0.1114	2.5929
SDI-III-0.4-0.4	0.1765	0.1187	0.8553	1.6885
SDI-I-0.5-0.5	0.1743	0.0485	0.1392	2.5239
SDI-II-0.5-0.5	0.1455	0.0515	0.0835	2.9344
SDI-III-0.5-0.5	0.1028	0.0833	0.9224	1.7512
SDI-I-0.6-0.6	0.1818	0.0371	0.1583	2.6535
SDI-II-0.6-0.6	0.0405	0.0201	0.0333	4.5719
SDI-III-0.6-0.6	0.0536	0.0547	0.6975	1.7938

Table 4. Optimization results for SDI-equipped structure under Northridge ground motion.

Control case	Optimization results			
	μ	λ	κ	γ_d
SDI-I-0.4-0.4	0.2781	0.0627	0.2106	1.6892
SDI-II-0.4-0.4	0.2478	0.0486	0.1125	2.5803
SDI-III-0.4-0.4	0.2097	0.0882	0.7987	1.6768
SDI-I-0.5-0.5	0.2791	0.0343	0.2153	2.3101
SDI-II-0.5-0.5	0.1994	0.0279	0.1090	3.0596
SDI-III-0.5-0.5	0.1281	0.0611	0.9254	1.7262
SDI-I-0.6-0.6	0.1885	0.0169	0.1305	2.9580
SDI-II-0.6-0.6	0.0245	0.0100	0.0194	5.1160
SDI-III-0.6-0.6	0.0524	0.0373	0.7483	1.7575

Table 5. Optimization results for SDI-equipped structure under Kobe ground motion.

Control case	Optimization results			
	μ	λ	κ	γ_d
SDI-I-0.4-0.4	0.5009	0.0847	0.4680	1.4673
SDI-II-0.4-0.4	0.3020	0.0710	0.0782	1.8524
SDI-III-0.4-0.4	0.2988	0.1016	0.9997	1.4574
SDI-I-0.5-0.5	0.2186	0.0414	0.1935	2.0827
SDI-II-0.5-0.5	0.1367	0.0347	0.0674	2.5682
SDI-III-0.5-0.5	0.1220	0.0552	0.9778	1.6841
SDI-I-0.6-0.6	0.1401	0.0253	0.1319	2.6198
SDI-II-0.6-0.6	0.0420	0.0120	0.0299	4.3411
SDI-III-0.6-0.6	0.0638	0.0352	0.8712	1.7485

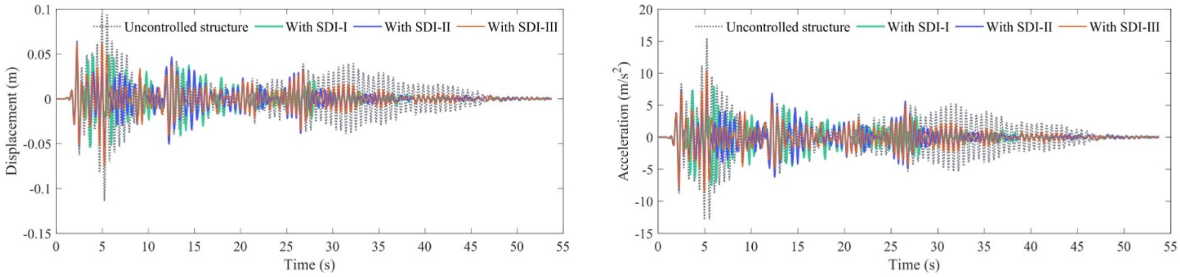

(a) Relative displacement response (b) Absolute acceleration response

Figure 14. Responses of structure with SDI systems under El Centro ground motion ($\gamma_{u,t} = 0.6$ and $\gamma_{a,t} = 0.6$).

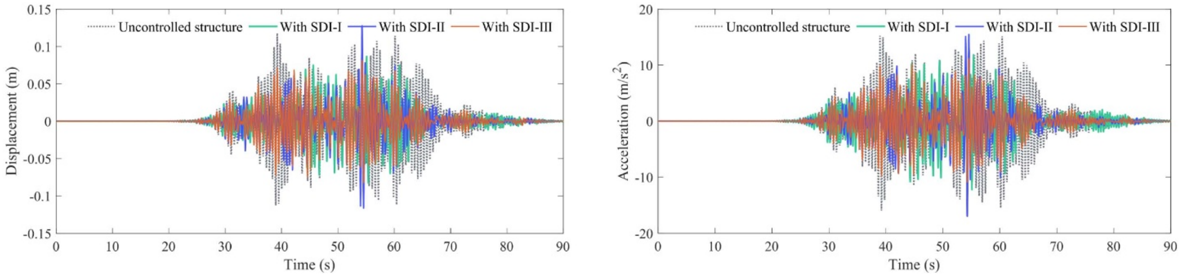

(a) Relative displacement response (b) Absolute acceleration response

Figure 15. Responses of structure with SDI systems under Chi–Chi ground motion ($\gamma_{u,t} = 0.6$ and $\gamma_{a,t} = 0.6$).

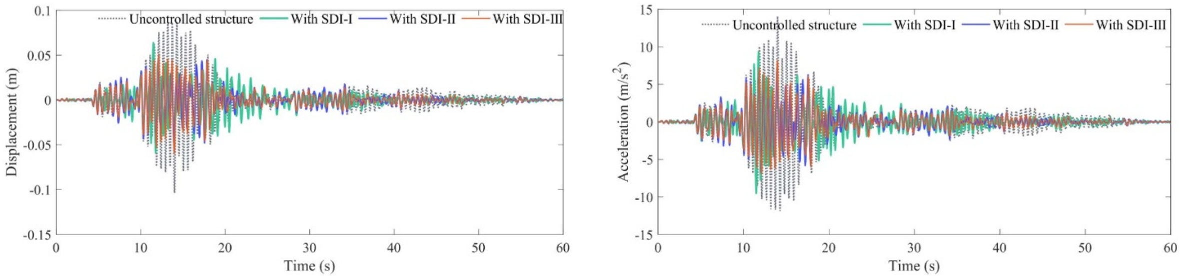

(a) Relative displacement response (b) Absolute acceleration response

Figure 16. Responses of structure with SDI systems under Northridge ground motion ($\gamma_{u,t} = 0.6$ and $\gamma_{a,t} = 0.6$).

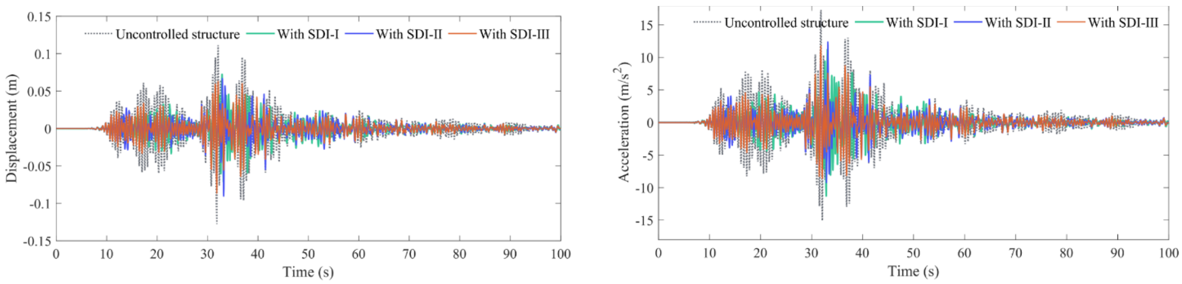

(a) Relative displacement response (b) Absolute acceleration response

Figure 17. Responses of structure with SDI systems under Kobe ground motion ($\gamma_{u,t} = 0.6$ and $\gamma_{a,t} = 0.6$).

different types of ground motions, the energy dissipation capacity of the SDI system is almost identical. In terms of different types of SDI system, the energy dissipation capacity among SDI systems shows similar behavior.

To illustrate the energy dissipation characteristic of the SDI-equipped structures more intuitively, the hysteretic curves of the SMA under different types of ground motion are depicted in figure 18. It can be observed that the energy dissipation

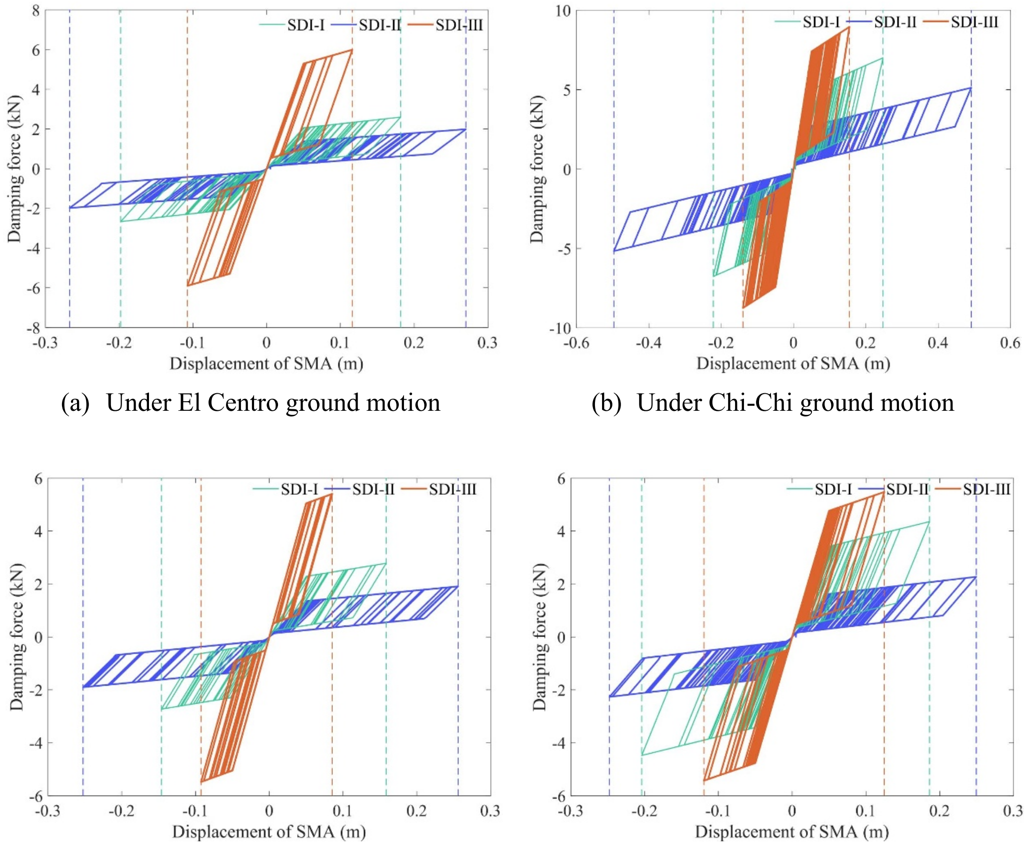

(a) Under El Centro ground motion

(b) Under Chi-Chi ground motion

(c) Under Northridge ground motion

(d) Under Kobe ground motion

Figure 18. Hysteretic curves of the SMA in SDI systems under different ground motions ($\gamma_{u,t} = 0.6$ and $\gamma_{a,t} = 0.6$).

Table 6. Results of γ_E under control cases in section 4.1.

Control case	El Centro	Chi–Chi	Northridge	Kobe
SDI-I-0.4-0.4	0.81	0.79	0.81	0.84
SDI-II-0.4-0.4	0.86	0.83	0.84	0.87
SDI-III-0.4-0.4	0.86	0.84	0.84	0.86
SDI-I-0.5-0.5	0.69	0.73	0.72	0.79
SDI-II-0.5-0.5	0.77	0.78	0.74	0.80
SDI-III-0.5-0.5	0.76	0.76	0.76	0.79
SDI-I-0.6-0.6	0.61	0.65	0.60	0.72
SDI-II-0.6-0.6	0.63	0.67	0.65	0.68
SDI-III-0.6-0.6	0.64	0.64	0.65	0.68

characteristic of the SDI systems differs although the energy dissipation ratio shows little difference as shown in table 6. The SDI-III generates a larger damping force with a relatively smaller deformation whereas the SDI-II exhibits a larger deformation with a relatively smaller damping force, which is in agreement with the discussion in section 4.2. In other words, the damping force of the SDI-II is smaller in comparison with other SDI systems, indicating that the damping enhancement effect of SDI-II performs better than the other SDI systems. On the other hand, it also implies that less material demand of SMA can be achieved in SDI-II with the overall energy dissipation capacity almost similar to other SDI systems.

5. Conclusions

Different mechanical layouts of SDI for structural response control are proposed and investigated in this study. A parameter comparative study is carried out by several performance indices, such as displacement response mitigation ratio, acceleration response mitigation ratio, and damping deformation enhancement ratio. An optimal design method for determining the parameters of the SDI systems based on fully utilizing the damping enhancement effect is proposed. The main conclusions drawn from this study can be summarized as follows:

(a) Different mechanical layouts of the SDI can lead to different control characteristics even the input parameters are all the same. Parameter analysis results obtained in this study can motivate appropriate selection for SDI mechanical layout: under the conditions that the stiffness ratio κ takes a smaller value (when the stiffness of the support is small), SDI-II exhibits to be more effective in reducing the structural responses. For a larger κ situation (when the stiffness of the support is large), SDI-III is found to be more effective.
(b) Using the proposed optimal design method, the damping enhancement effect of the SDI systems is fully utilized, in other words, the energy dissipation capacity of SMA

is fully developed and less material demand of SMA can therefore be achieved. Meanwhile, the displacement and acceleration responses of the SDI-equipped structures can be simultaneously effectively mitigated.

(c) In terms of energy dissipation capacity, the optimized SDI systems show similar behavior. However, the energy dissipation characteristic differs, that is, the SDI-III system generates a larger damping force with a relatively smaller deformation whereas the SDI-II exhibits a larger deformation with a relatively smaller damping force. In other words, with almost identical energy dissipation capacity of the three SDI systems, the damping force of SDI-II is smaller, indicating that the damping enhancement effect of SDI-II performs better than the other SDI systems. It also implies that less material demand of SMA can be achieved in SDI-II.

(d) The detailed realization difficulties of the SDI systems such as the actual space to allocate the SDI systems and the material cost of the SDI systems are important issues for practical application. To address these issues, experimental tests for the SDI systems will be investigated in the future. Additionally, it is promising for future studies to extend the current work to structural vibration control with other smart materials and SDI systems.

Data availability statement

All data that support the findings of this study are included within the article (and any supplementary files).

Acknowledgment

This study was supported by the National Natural Science Foundation of China (Grant No. 51978525), Scientific Research Fund of Institute of Engineering Mechanics, China Earthquake Administration (Grant No. 2020EEEVL0401, 2019EEVL03 and 2019D14), Shanghai Committee of Science and Technology, China (Grant No. 19DZ1202500) and Shaanxi Provincial Key Research and Development Program (Grant No. 2021GY-314).

ORCID iDs

Ruifu Zhang https://orcid.org/0000-0003-2988-4412
Jieling Jiang https://orcid.org/0000-0003-0961-2727
Yingqi Jia https://orcid.org/0000-0002-3541-5535
Chao Wang https://orcid.org/0000-0002-0347-7256

References

[1] Housner G W, Bergman L A, Caughey T K, Chassiakos A G, Claus R O, Masri S F, Skelton R E, Soong T T, Spencer B F and Yao J T P 1997 Structural control: past, present, and future *J. Eng. Mech.* **123** 897–971
[2] Spencer B, Nathan M and Nagarajaiah S 2003 State of the art of structural control *J. Struct. Eng.* **129** 845–56
[3] Li C, Chang K, Cao L and Huang Y 2021 Performance of a nonlinear hybrid base isolation system under the ground motions *Soil Dyn. Earthq. Eng.* **143** 106589
[4] Kitagawa Y and Midorikawa M 1998 Seismic isolation and passive response-control buildings in Japan *Smart Mater. Struct.* **7** 581–7
[5] Soong T T and Spencer B F 2002 Supplemental energy dissipation: state-of-the-art and state-of-the practice *Eng. Struct.* **24** 243–59
[6] Saaed T, Nikolakopoulos G, Jonasson J E and Hedlund H 2013 A state-of-the-art review of structural control systems *J. Vib. Control* **21** 919–37
[7] Pan C, Zhang R F, Luo H, Li C and Shen H 2018 Demand-based optimal design of oscillator with parallel-layout viscous inerter damper *Struct. Control Health Monit.* **25** e2051
[8] Ikago K, Saito K and Inoue N 2012 Seismic control of single-degree-of-freedom structure using tuned viscous mass damper *Earthq. Eng. Struct. Dyn.* **41** 453–74
[9] Parulekar Y M, Reddy G R, Vaze K K, Guha S, Gupta C, Muthumani K and Sreekala R 2012 Seismic response attenuation of structures using shape memory alloy dampers *Struct. Control Health Monit.* **19** 102–19
[10] Song G, Ma N and Li H N 2006 Applications of shape memory alloys in civil structures *Eng. Struct.* **28** 1266–74
[11] Dolce M, Cardone D and Marnetto R 2000 Implementation and testing of passive control devices on shape memory alloys *Earthq. Eng. Struct. Dyn.* **29** 945–68
[12] Naresh C, Bose P S C and Rao C 2016 Shape memory alloys: a state of art review *IOP Conf. Ser.: Mater. Sci. Eng.* **149** 012054
[13] Choi E, Mohammadzadeh B and Kim H 2018 SMA bending bars as self-centering and damping devices *Smart Mater. Struct.* **28** 025029
[14] Jia Y Q, Lu Z D, Li L Z and Wu Z L 2018 A review of applications and research of shape memory alloys in civil engineering *IOP Conf. Ser.: Mater. Sci. Eng.* **392** 022009
[15] Huang H, Mosalam K M and Chang W-S 2020 Adaptive tuned mass damper with shape memory alloy for seismic application *Eng. Struct.* **223** 111171
[16] Li H N, Liu M M and Fu X 2018 An innovative re-centering SMA-lead damper and its application to steel frame structures *Smart Mater. Struct.* **27** 075029
[17] Silwal B, Michael R J and Ozbulut O E 2015 A superelastic viscous damper for enhanced seismic performance of steel moment frames *Eng. Struct.* **105** 152–64
[18] Mishra S, Gur S and Chakraborty S 2013 An improved tuned mass damper (SMA-TMD) assisted by a shape memory alloy spring *Smart Mater. Struct.* **22** 095016
[19] Parulekar Y M, Kiran A R, Reddy G R, Singh R K and Vaze K K 2014 Shake table tests and analytical simulations of a steel structure with shape memory alloy dampers *Smart Mater. Struct.* **23** 125002
[20] Qian H, Li H N and Song G B 2016 Experimental investigations of building structure with a superelastic shape memory alloy friction damper subject to seismic loads *Smart Mater. Struct.* **25** 14
[21] Qiu C X, Fang C, Liang D, Du X L and Yam M C H 2020 Behavior and application of self-centering dampers equipped with buckling-restrained SMA bars *Smart Mater. Struct.* **29** 16
[22] Li H, Mao C and Ou J-P 2008 Experimental and theoretical study on two types of shape memory alloy devices *Earthq. Eng. Struct. Dyn.* **37** 407–26
[23] Zhang Z H, Bi K M, Hao H, Sheng P, Feng L and Xiao D 2020 Development of a novel deformation-amplified shape memory alloy-friction damper for mitigating seismic responses of RC frame buildings *Eng. Struct.* **216** 19

[24] Zhang R F, Zhao Z P, Pan C, Ikago K and Xue S T 2020 Damping enhancement principle of inerter system *Struct. Control Health Monit.* **27** e2523
[25] Pan C and Zhang R F 2018 Design of structure with inerter system based on stochastic response mitigation ratio *Struct. Control Health Monit.* **25** e2169
[26] Kawamata S 1973 *Development of a Vibration Control System of Structures by Means of Mass Pumps* (Tokyo: Institute of Industrial Science, University of Tokyo)
[27] Ikago K, Sugimura Y, Saito K and Inoue N 2010 Optimum seismic response control of multiple degree of freedom structures using tuned viscous mass dampers *Proc. 10th Int. Conf. on Computational Structures Technology* (*Valencia, Spain*)
[28] Saito K, Sugimura Y and Inoue N 2008 A study on response control of a structure using viscous damper with inertial mass *J. Struct. Eng.* **B54** 635–48
[29] Arai T, Aburakawa T, Ikago K, Hori N and Inoue N 2009 Verification on effectiveness of a tuned viscous mass damper and its applicability to non-linear structural systems *J. Struct. Constr. Eng.* **74** 1993–2002
[30] Jia Y Q, Li L Z, Wang C, Lu Z D and Zhang R F 2019 A novel shape memory alloy damping inerter for vibration mitigation *Smart Mater. Struct.* **28** 115002
[31] Das S, Chakraborty A and Barua I 2020 Optimal tuning of SMA inerter for simultaneous wind induced vibration control of high-rise building and energy harvesting *Smart Mater. Struct.* **30** 025027
[32] Tiwari N D, Gogoi A, Hazra B and Wang Q 2021 A shape memory alloy-tuned mass damper inerter system for passive control of linked-SDOF structural systems under seismic excitation *J. Sound Vib.* **494** 115893
[33] Zhao Z P, Chen Q J, Zhang R F, Jiang Y Y and Pan C 2020 A negative stiffness inerter system (NSIS) for earthquake protection purposes *Smart Struct. Syst.* **26** 481–93
[34] Yan X and Nie J X 2000 Response of SMA superelastic systems under random excitation *J. Sound Vib.* **238** 893–901
[35] Graesser E and Cozzarelli F 1991 Shape memory alloys as new materials for aseismic isolation *J. Eng. Mech.* **117** 2590–608
[36] Gur S, Mishra S K and Roy K 2016 Stochastic seismic response of building with super-elastic damper *Mech. Syst. Signal Process.* **72–73** 642–59
[37] Hieu D V, Hai N and Hung D 2018 The equivalent linearization method with a weighted averaging for solving undamped nonlinear oscillators *J. Appl. Math.* **2018** 1–15
[38] Lin J H, Zhang Y, Li Q and Williams F W 2004 Seismic spatial effects for long-span bridges using the pseudo excitation method *Eng. Struct.* **26** 1207–16
[39] Silva C 2005 *Vibration and Shock Handbook* (Boca Raton: CRC Press) (https://doi.org/10.1201/9781420039894)
[40] Lin J, Zhang W and Williams F 1994 Pseudo-excitation algorithm for nonstationary random seismic responses *Eng. Struct.* **16** 270–6
[41] Clough R W and Penzien J 2003 *Dynamics of Structures* 3rd edn (Berkeley, CA: Computers and Structures Inc)
[42] Kanai K 1957 Semi-empirical formula for the seismic characteristics of the ground *Bull. Earthq. Res. Inst. Japan* **35** 281–4
[43] Ha T 1960 A statistical method of determining the maximum response of a building structure during an earthquake *Proc. 2nd World Conf. on Earthquake Engineering* p A-2
[44] Lopez-Garcia D and Soong T T 2009 Assessment of the separation necessary to prevent seismic pounding between linear structural systems *Probabilistic Eng. Mech.* **24** 210–23
[45] Li C and Liu Y 2004 Ground motion dominant frequency effect on the design of multiple tuned mass dampers *J. Earthq. Eng.* **8** 89–105
[46] Chopra A K 2012 *Dynamics of Structures: Theory and Applications to Earthquake Engineering* 4th edn (New York: Prentice Hall)
[47] Matheworks. MATLAB R2019a (available at: https://ww2.mathworks.cn/2019)
[48] Suman B 2003 Simulated annealing-based multiobjective algorithms and their application for system reliability *Eng. Optim.* **35** 391–416
[49] Chen Q J, Zhao Z P, Zhang R F and Pan C 2018 Impact of soil-structure interaction on structures with inerter system *J. Sound Vib.* **433** 1–15
[50] Ancheta T D, Darragh R B and Stewart P J 2013 Pacific earthquake engineering research center (PEER)